Sulfur Impregnation in Polypyrrole-Modified MnO_2 Nanotubes: Efficient Polysulfide Adsorption for Improved Lithium-Sulfur Battery Performance

Pengcheng Du[#*a], Wenli Wei[#ab], Yuman Dong[#a], Dong Liu[a], Qi Wang[a], Peng Yi[b] Shaowei Chen*[b], Peng Liu*[a]

[a] *State Key Laboratory of Applied Organic Chemistry and Institute of Polymer Science and Engineering, College of Chemistry and Chemical Engineering, Lanzhou University, Lanzhou 730000, People's Republic of China*
[b] *Department of Chemistry and Biochemistry, University of California, 1156 High Street, Santa Cruz, California 95064, USA*
[#] *These authors contributed equally to this work.*

Abstract:

Rechargeable lithium-sulfur batteries have emerged as a viable technology for next generation electrochemical energy storage, and the sulfur cathode plays a critical role in determining the device performance. In this study, we prepared functional composites based on polypyrrole-coated MnO_2 nanotubules as a highly efficient sulfur host (sulfur mass loading 71%). The hollow interior of the MnO_2 nanotubes not only allowed for accommodation of volumetric changes of sulfur particles during the cycling process, but also confined the diffusion of lithium polysulfides by physical restriction and chemical adsorption, which minimized the loss of polysulfide species. In addition, the polypyrrole outer layer effectively enhanced the electrical conductivity of the cathode to facilitate ion and electron transport. The as-prepared MnO_2-PPy-S composite delivered an initial specific capacity of 1469 mAh/g and maintained an extremely stable cycling performance, with a small capacity decay of merely 0.07% per cycle at 0.2 C within 500 cycles, a high average coulombic efficiency of 95.7% and an excellent rate capability at 470 mAh/g at the current density of 5 C.

Keywords: *MnO_2 nanotube, polypyrrole, polysulfide, lithium-sulfur battery*

1. Introduction

Lithium sulfur batteries (LSB) have been attracting extensive interest as a promising next-generation high energy storage technology, due to the high theoretical specific capacity, low costs and environmental friendliness of the electrode materials [1-4]. Sulfur has been known to undergo multi-electron reactions with Li ions and exhibit a high theoretical specific capacity of 1672 mAh/g [4]. Ideally, the cathode materials for LSB should include a high surface area and large pore volume to accommodate a high loading of sulfur particles, strong polar absorption for soluble reactive intermediates, and highly conductive network for rapid transport of ions and electrons [5]. However, the performance of LSB has been limited by several challenging obstacles, such as fast capacity decay, low coulombic efficiency and poor rate capability, which greatly hinder the practical applications [3,4]. These issues are mainly ascribed to the low electrical conductivity of the active materials (e.g., sulfur, Li_2S, and Li_2S_2), diffusion (and loss) of soluble polysulfide intermediates, and large volumetric changes of the cathode materials during the charge-discharge process.

These issues may be mitigated by the development of new, effective sulfur hosts [6,7], modification of membrane surfaces [8-10], and/or addition of electrolyte additives [11,12]. In a number of studies, conductive matrices, such as carbon materials and conductive polymers, have been employed to encapsulate sulfur, improve electrical conductivity of the cathode as well as minimize the loss of lithium polysulfides [13,14]. In particular, carbon materials with a high specific surface area and large pore volume have been used rather extensively, such as meso/microporous carbons [15], graphene [6,16-18], hollow

carbon nanofibers [19], hollow carbon nanospheres [20], and carbon nanotubes [21,22]. In addition, conductive polymers, such as polypyrrole (PPy) [23], polyaniline (PANI) [24] and poly(3,4-ethylenedioxythiophne) (PEDOT) [7,25], have also been used to host sulfur particles. The resulting sulfur-encapsulated nanocomposites typically exhibit enhanced specific capacity and good cycling performance during the initial cycles. But the coulombic efficiency in general remains low, and rapid capacity loss occurs during long-term cycling, as the non-polar carbon/polymer hosts cannot efficiently entrap the polar lithium polysulfide species because of weak interactions with sulfur.

Polar host materials, such as metal oxides of TiO_2 [26] and MnO_2 [27], metal hydroxides of $Ni(OH)_2$ [28], and metal-organic frameworks (MOFs) [29,30], have been found to form strong chemical bonds with lithium polysulfides, which can significantly improve the long-term cycling performance of LSB. Of these, MnO_2-based nanocomposites with a uniform structure and large surface area have been attracting particular attention [31]. For instance, Nazar and coworkers dispersed sulfur onto the surface of MnO_2 nanosheets [32] and then covered the sulfur with a MnO_2 shell [27] to improve the electrochemical performance. In another study [33], Chen's group decorated hollow sulfur nanospheres with MnO_2 nanosheets. Diao and coworkers synthetized unique sulfur/γ-MnO_2 core-shell nanocomposites [34]. However, the electrical conductivity of these metal-oxide materials is typically low, in comparison with carbon and conductive polymers, which compromises the rate capability and specific capacity of LSB. Consequently, conductive additives are generally added to the cathode materials. This inevitably reduces the mass loading of active sulfur.

Therefore, it can be envisaged that nanocomposites based on the combination of conductive matrices and polar metal oxides may serve as effective host materials of sulfur. For instance, Lou and coworkers fabricated hollow carbon nanofibers filled with MnO_2 nanosheets to host sulfur nanoparticles [35]. Kong's group used hollow MnO_2 nanospheres with a PPy shell to encapsulate sulfur, which exhibited an excellent cycling performance [36]. Yu's group also synthesized PPy-MnO_2 nanotubes as a sulfur host for high-performance lithium sulfur batteries [37] .

In this work, we prepared PPy-modified MnO_2 nanotubes for effective encapsulation of sulfur nanoparticles. The MnO_2 nanotubes were synthesized through a facile hydrothermal method and the PPy layer was formed in situ by using the MnO_2 as the oxidant. Sulfur nanoparticles were then melted and diffused into the nanotubes. The resulting ternary structure exhibited at least two advantages. First, the hollow interior of the MnO_2 nanotubes provided a large space for the loading of sulfur particles, and the strong chemical interactions with polysulfides intermediates helped minimize the loss of the active species. Second, the PPy shells efficiently enhanced the electrical conductivity of the cathode materials. These led to a remarkable performance as a LSB cathode material.

2. Experimental

2.1 Materials and reagents

Pyrrole was used after purification by distillation. Concentrated sulfuric acid (H_2SO_4) and hydrochloric acid (HCl) were purchased from Baiyin Liangyou Chemical Reagents Co., Ltd. Potassium permanganate ($KMnO_4$) were purchased from Guangfu

Chemical Reagents Co. Sublimed sulfur (99.95%) was obtained from Aladdin Industrial Corporation.

2.2 Fabrication of PPy-modified MnO_2 nanotube-sulfur composites

As shown in Scheme 1, MnO_2 nanotubes were first prepared by a facile hydrothermal method [38,39]. In brief, 0.658 g of $KMnO_4$ was dissolved in 75 mL of deionized water. Then 1.5 mL of concentrated HCl was added into the solution in a dropwise fashion under magnetic stirring for 15 min at ambient temperature. The solution was then transferred to a 100 mL Teflon-lined stainless autoclave, and heated at 150 °C for 12 h. After being cooled down to room temperature, brown precipitates (MnO_2 nanotubes) were filtered and washed with deionized water and ethanol, and then dried at 60 °C in an oven.

MnO_2-PPy nanotubes were then prepared by using the obtained MnO_2 nanotubes as reaction templates. Experimentally, 0.2 g of the as-prepared MnO_2 nanotubes was dispersed in 1 M HCl solution (50 mL) under sonication. After magnetic stirring for 30 min in an ice bath, 980 μL of pyrrole was added to the suspension, and the polymerization was carried out in the ice bath for 12 h. Dark blue precipitates were obtained by centrifugation, washed with deionized water and ethanol several times, and then dried at 60 °C, affording MnO_2-PPy nanotubes.

The obtained MnO_2-PPy nanotubes were then homogeneously blended with sulfur as a mass ratio of 3:7, and the mixture was heated at 155 °C for 24 h in a nitrogen atmosphere, such that sulfur was melted and infiltrate the hollow interiors of the MnO_2-PPy nanotubes. To remove sulfur on the outside surface of the MnO_2-PPy nanotubes,

the sample was heated at 200 °C for 2 h. The resulting sample was referred to as MnO_2-PPy-S.

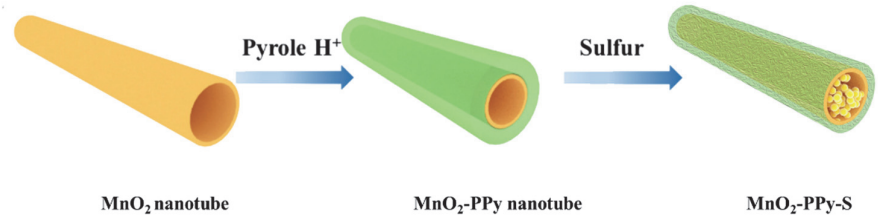

Scheme 1. Schematic illustration of the fabrication of PPy modified MnO_2 nanotube-sulfur composites.

2.3 Characterization

The surface morphology of the as-prepared nanocomposites was examined with a scanning electron microscope (SEM, Hitachi S-4800, Japan) equipped with energy dispersive X-ray spectroscopy (EDX), and a high-resolution transmission electron microscope (HR-TEM, JEOL TEM-2010). The sample crystallinity was characterized by using an X-ray diffractometer (XRD, Shimadzu Corp., Kyoto, Japan) with Cu K_α radiation. Thermogravimetric analysis (TGA) (TA Instruments, New Castle, DE) was carried out under a N_2 atmosphere at the heating rate of 10 °C/min.

2.4 Electrochemistry

To prepare working cathodes, the active material obtained above was blended with acetylene black as a conductive agent and polyvinylidenediuoride (PVDF) as binders, at the mass ratio of 7:2:1, in N-methyl-2-pyrrolidone (NMP) to form a uniform slurry. The slurry was cast onto an Al foil current collector and dried at 40 °C for 12 h in a vacuum oven. CR3032 half coin cells were assembled in a glove box filled with argon. Lithium foils were employed as both the counter and reference electrodes, the active

material as the cathode and a Celgard 2400 membrane as the separator. The liquid electrolyte was composed of 1 M bis(trifluoromethane) sulfonimide lithium salt (LiTFSI) dissolved in a mixture of 1.3-dioxolane (DOL) and dimethoxymethane (DME) (1:1 v:v) with 1% $LiNO_3$ additive. Electrochemical performance was tested at various current densities within the voltage range of 1.7 to 2.8 V versus Li^+/Li using a CT2001A battery testing system (LAND Electronic Co.). The electrodes were cycled with a CHI 660E electrochemical workstation in the potential window of 1.7 to 2.8 V versus Li^+/Li at the scan rate of 0.1 mV/s.

3. Results and Discussion

3.1 Structural Characterization

The structure of the nanotube nanocomposites was first characterized by SEM and TEM measurements. From the SEM images in Figure S1, it can be seen that the MnO_2 nanotubes exhibited a smooth surface morphology with an outer diameter of about 100 nm (Figure S1a), and the hollow tubular interior can be clearly identified in TEM measurements, with an inner diameter of about 70 nm (Figure 1a,b). After the coating of a PPy layer, the deposition of PPy nanoparticles rendered the MnO_2 nanotube surfaces drastically roughened, as shown in Figure S1b,c and Figure 1c,d. The formation of this rather compact PPy layer was likely due to the MnO_2 nanotubes that served both as a supporting scaffold and an oxidizing agent for pyrrole polymerization [37]. One can see that in the MnO_2-PPy samples, the hollow nanotube structure was retained, which may be exploited for the loading of sulfur. This can be clearly seen in TEM studies (Figure 1e, f), whereas no obvious sulfur particles were found on the

exterior of the MnO_2-PPy nanotubes (Figure S1d-f), suggesting efficient confinement of sulfur within the MnO_2 nanotubes. Indeed, EDS mapping analysis (Figure 2) shows that the elements of carbon, nitrogen, oxygen, sulfur and manganese were uniformly distributed throughout the sample, indicating the successful and homogeneous loading of PPy and sulfur into the MnO_2 nanotubes.

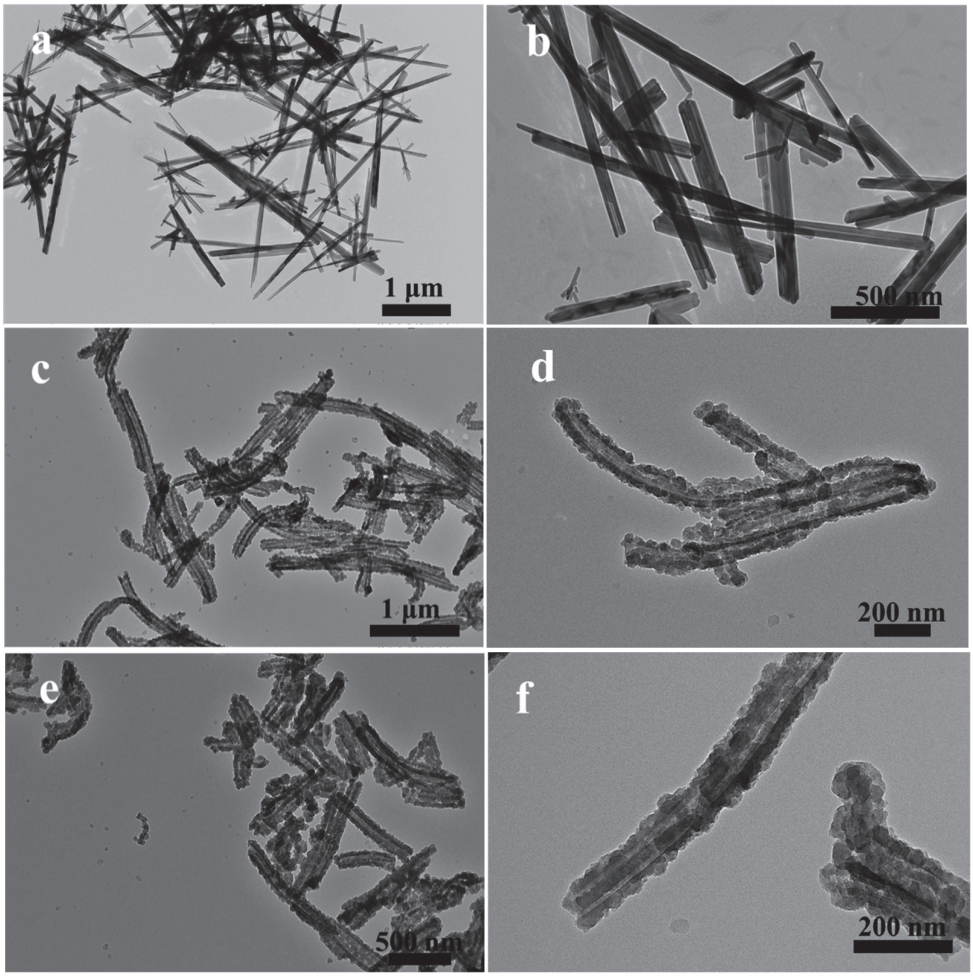

Figure 1. TEM images of (a, b) MnO_2 nanotubes, (c,d) MnO_2-PPy nanotubes, and (e,f) MnO_2-PPy-S.

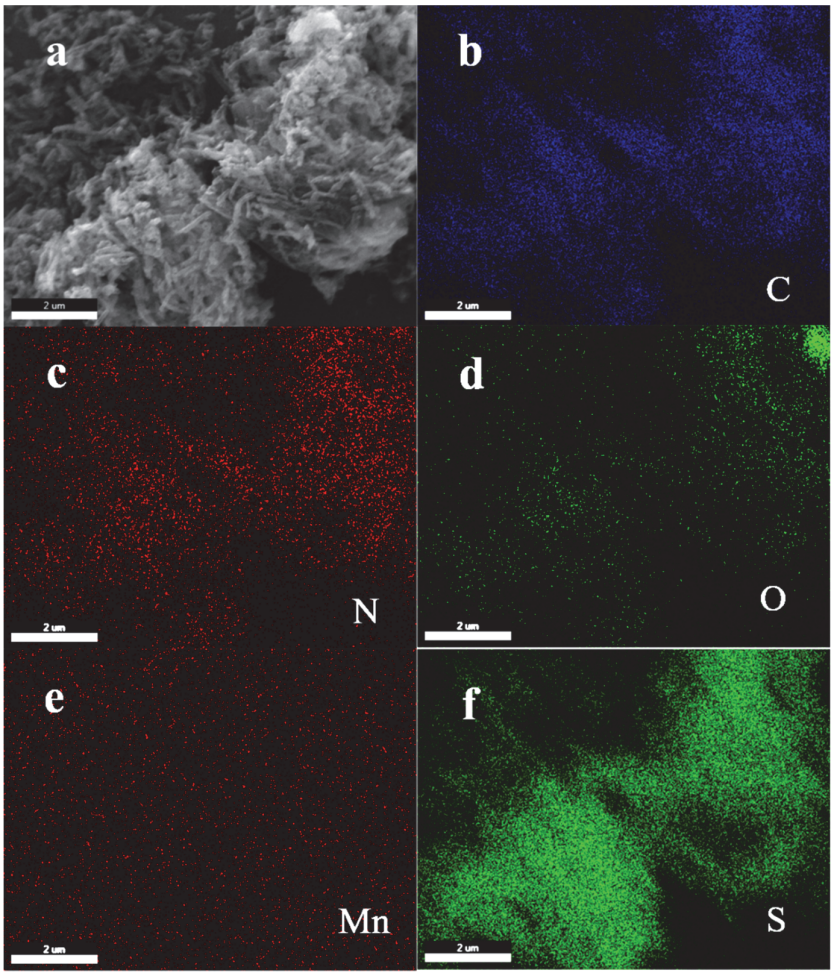

Figure 2. (a) SEM image of MnO_2-PPy-S and the corresponding elemental maps of (b) carbon, (c) nitrogen, (d) oxygen, (e) manganese and (f) sulfur. Scale bars 2 μm.

The crystalline structures of the samples were then examined by XRD measurements. As shown in Figure S2a, MnO_2 nanotubes exhibited a series of well-defined diffraction peaks at 12.6°, 18.1°, 28.8°, 37.6°, 41.9°, 49.9°, 56.2°, 60.2°, 65.1º and 69.7º, which can be ascribed, respectively, to the (110), (200), (310), (211), (301), (411), (521), (002) and (541) crystal planes of tetragonal-like α-MnO_2 (JCPDS NO. 44-0141); whereas MnO_2-PPy shows only a featureless profile except for a broad peak at ca. 24.4°, [23] suggesting an amorphous structure of a PPy outer layer. Interestingly, the diffraction patterns of the MnO_2-PPy-S composite were dominated by those of sulfur, likely because of the high loading of sulfur.

Consistent results were obtained in FT-IR measurements. From Figure S2b, it is obvious that MnO_2-PPy exhibited a spectral profile consistent with that of PPy, indicating that the MnO_2 nanotubes were well coated with PPy layers. The characteristic bands at 1550 cm^{-1} and 1458 cm^{-1} can be ascribed to the fundamental vibrations of the polypyrrole ring, the bands at 1290 cm^{-1} and 1045 cm^{-1} are due to the C-H in-plane vibrations, and the band at 1180 cm^{-1} arises from the C-N stretching vibration of the polypyrrole chain [40-42]. Interestingly, after sulfur loading, these vibrational features became less well-defined for the MnO_2-PPy-S sample [36].

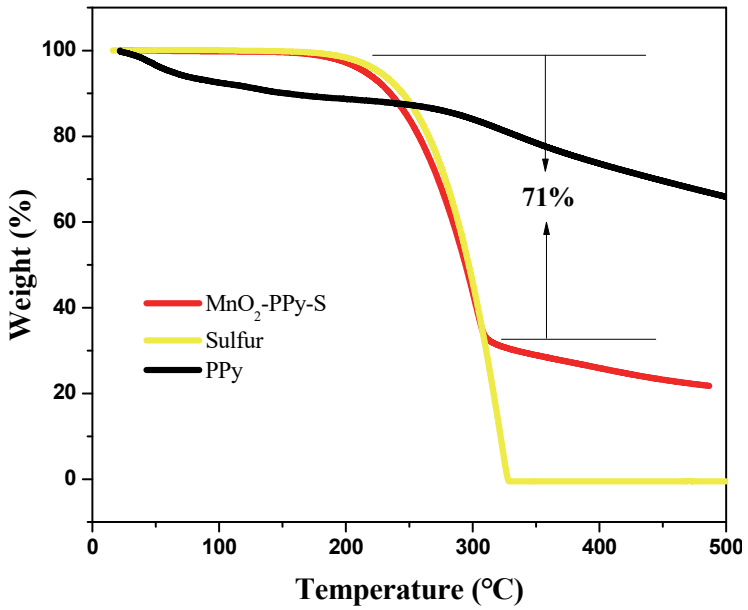

Figure 3. TGA curves of PPy, pure sulfur and MnO_2-PPy-S.

The loading of sulfur in the MnO_2-PPy-S composite was then quantitatively evaluated by TGA measurements. From Figure 3, one can see that the weight loss of the MnO_2-PPy-S sample commenced at ca. 180 °C, and the sample weight remained virtually unchanged at temperatures over ca. 310 °C. This profile is very similar to that of pure sulfur, whereas PPy was rather stable within this temperature range. The total weight loss for MnO_2-PPy-S was estimated to be 71%. That is, sulfur accounts for about

71% of the MnO_2-PPy-S sample weight.

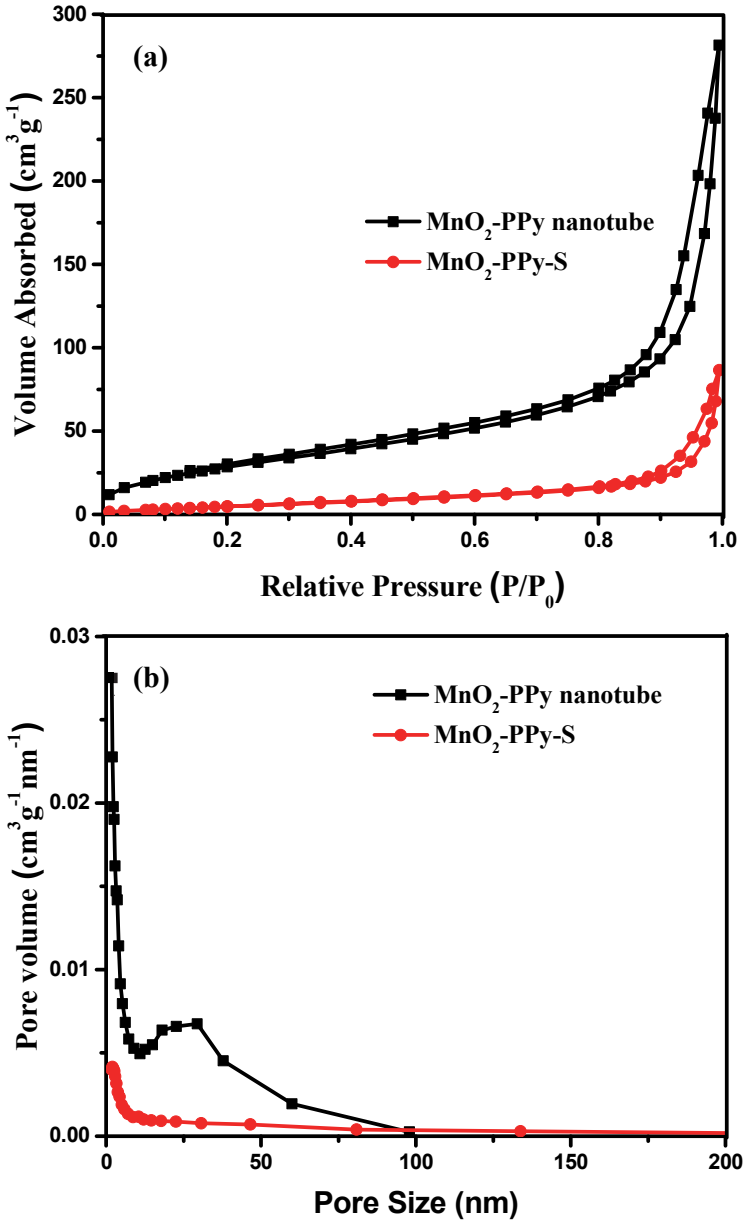

Figure 4. (a) N_2 adsorption–desorption isotherms and (b) size distribution of MnO_2-PPy and MnO_2-PPy-S.

N_2 adsorption-desorption measurements were then carried out to quantify the specific surface area and pore structure of the MnO_2-PPy and MnO_2-PPy-S nanocomposites. From Figure 4a, it can be seen that both samples exhibited type IV adsorption isotherms, indicative of the formation of mesoporous structures. The BET

surface area of the MnO_2-PPy was calculated to be 111.51 m^2/g, which diminished markedly to 21.46 m^2/g for MnO_2-PPy-S as sulfur impregnated the MnO_2 hollow tubes. The mesoporous size distributions of the samples are shown in Figure 4b. The MnO_2-PPy showed a pore volume of 0.44 cm^2/g with an average pore size of 13.87 nm, while after sulfur loading, the MnO_2-PPy-S sample displayed a substantial decrease of the pore volume to 0.13 cm^2/g, whereas the average pore size increased to 19.16 nm, likely because smaller pores were easier to fill up with sulfur impregnation.

3.2 Electrochemical performance

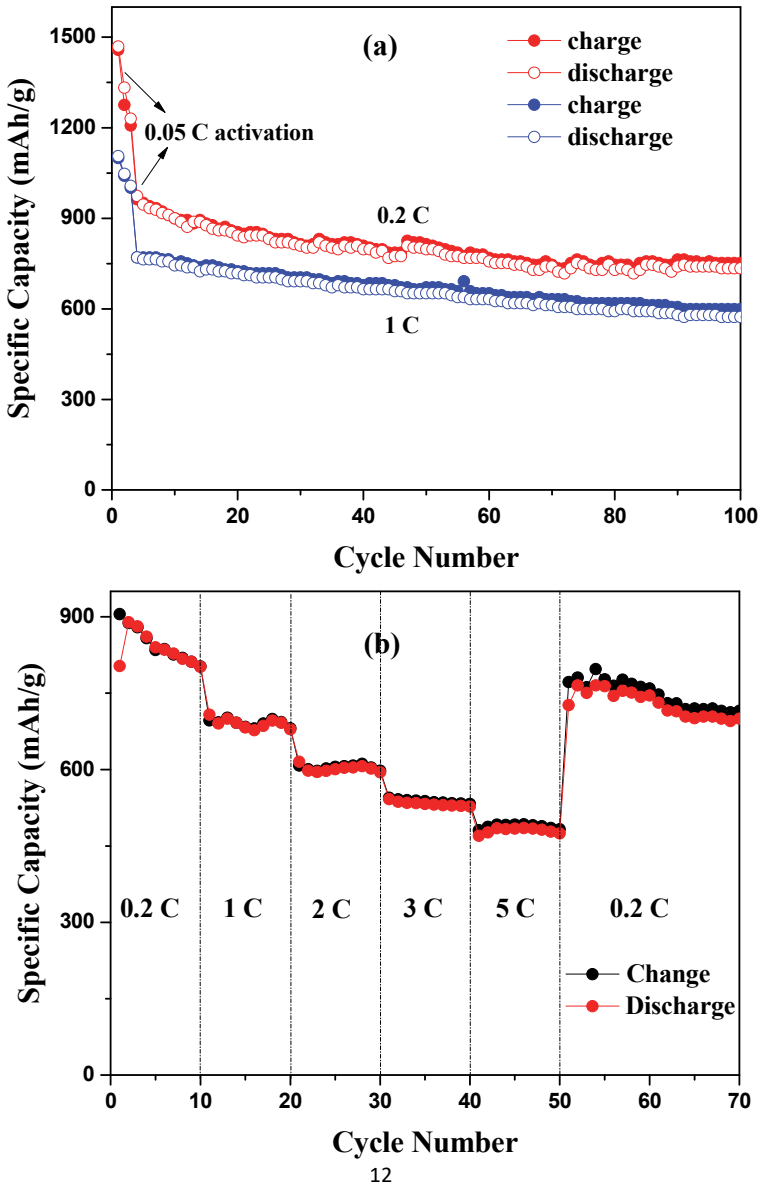

Figure 5. (a) Cycling stability and (b) rate capacities of the MnO_2-PPy-S composites of the MnO_2-PPy-S composites at different current densities.

The performance of the MnO_2-PPy-S composite as a cathode material for LSB was then evaluated electrochemically. Figure 5a shows the charging-discharging cycling performance of the sample at different current densities. The electrode was first cycled at a low current density of 0.05 C for activation and then charged and discharged at the current density of 0.2 C and 1 C, respectively. After activation for three cycles, the cathode delivered a specific capacity of 973.8 mAh/g at 0.2 C and 770.4 mAh/g at 1 C, respectively; and after 100 cycles, the capacity remained promising at 734.6 and 572.8 mAh/g.

To evaluate the rate capability of the MnO_2-PPy-S composites, the electrode was charged and discharged from 0.2 C to 1 C, 2 C, 3 C, 5 C and finally back to 0.2 C at the voltage range of 0.01 V-3 V, as shown in Figure 5b. The initial specific discharge capacity was 803.3 mAh/g at 0.2 C, and then decreased slowly to 708.0 mAh/g at 1 C, 615.3 mAh/g at 2 C, 542.0 mAh/g at 3 C, and 470.0 mAh/g at 5 C. More importantly, the electrode was able to deliver a specific capacity of 726.6 mAh/g when the current density was re-increased to 0.2 C, more than 90% retention as compared to the initial specific capacity. This suggests high reversibility of the operation.

The durability of the MnO_2-PPy-S electrode was further examined by charging and discharging at the current density of 0.2 C for 500 cycles. From Figure 6a (left y axis), one can see that during the initial activation at 0.05 C, the electrode delivered a specific capacity of 1469.2 mAh/g in the first cycle. Then as the current density increased to 0.2 C, the specific discharge capacity diminished to 973.8 mAh/g in the

4th cycle. In the following cycles, the discharge capacity declined much more slowly to 734.6 mAh/g in the 100th cycle, 694.8 mAh/g in the 200th, 671.9 mAh/g in the 300th, and 632.1 mAh/g in the 400th cycle and remained almost invariant at around 586 mAh/g after the 500th cycle. This means that on average there was only 0.07 % capacity decay per cycle during this discharge-charge process (Figure 6b). Consistent behaviors can be observed with the corresponding coulombic efficiency (Figure 8a, right y axis), where the MnO_2-PPy-S electrode can be seen to demonstrate an outstanding coulombic efficiency of 95.7 % on average.

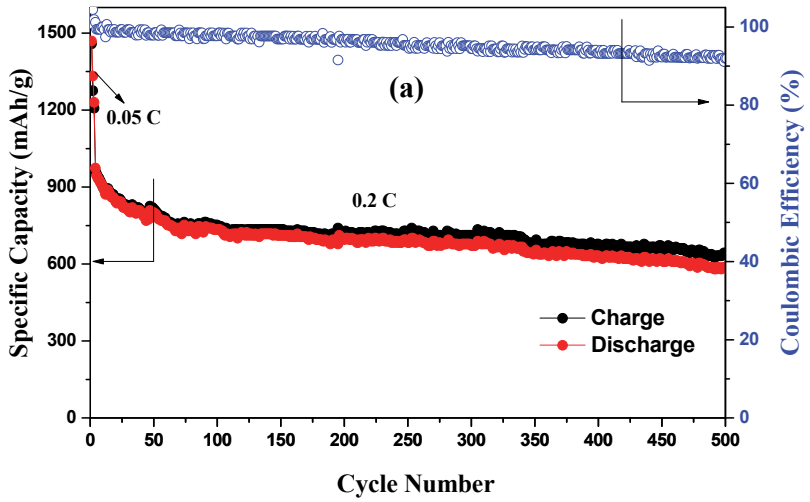

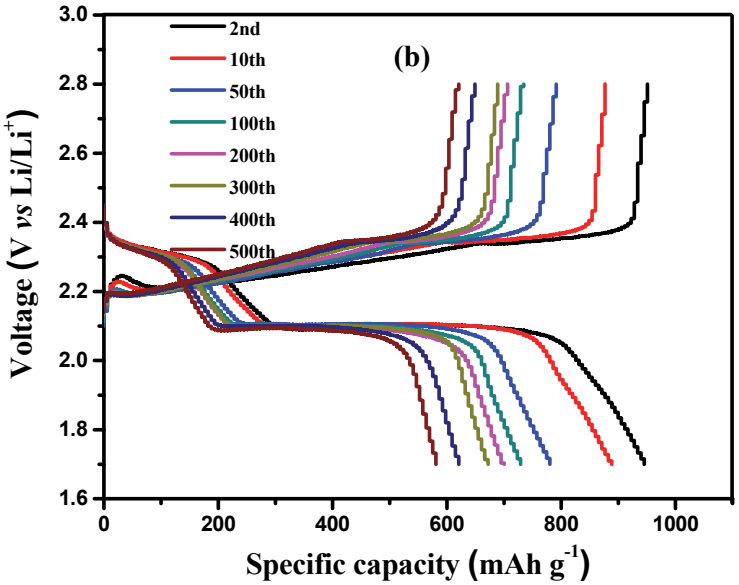

Figure 6. (a) Cycling capacity at 0.2 C-rate and the corresponding coulombic efficiency of the MnO_2-PPy-S composites and (b) cycling charge-discharge profiles of MnO_2-PPy-S composites at 0.2 C rate.

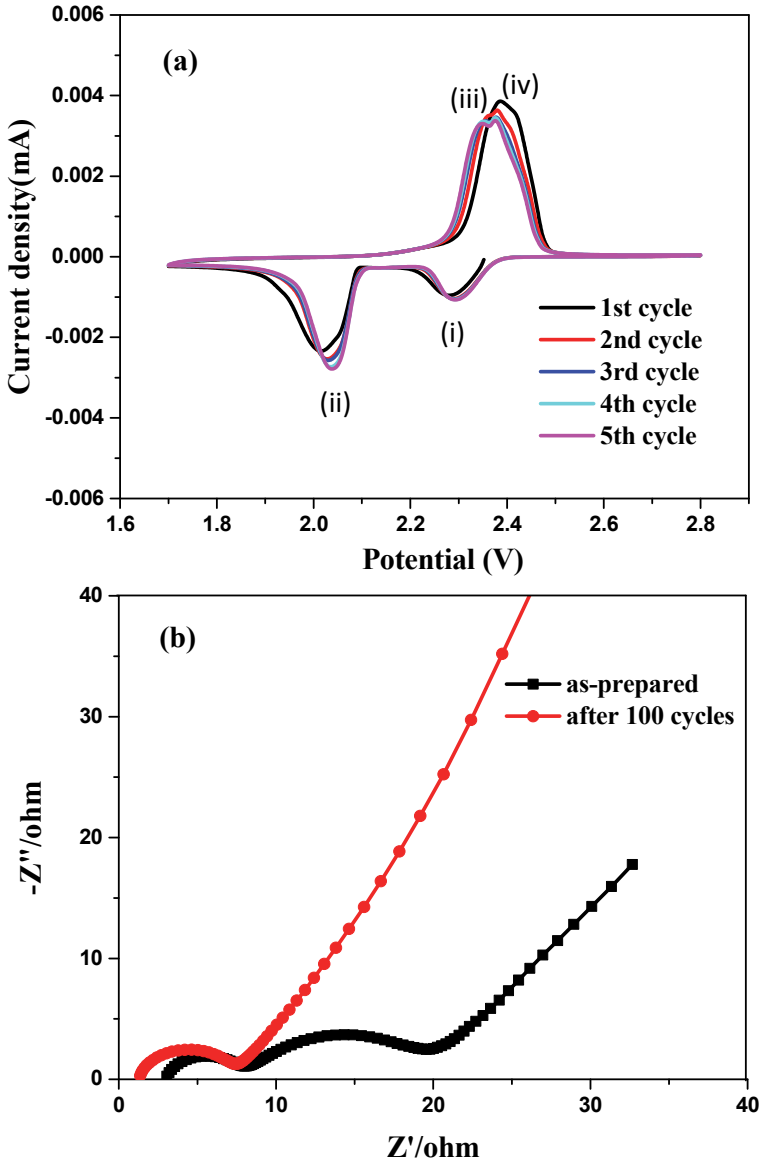

Figure 7. (a) Cyclic voltammograms of the MnO_2-PPy-S composites at the scan rate of 0.1 mV/s. (b) Nyquist plots of the MnO_2-PPy-S composites before and after 100 cycles.

To evaluate the electrochemical reaction mechanism, the MnO_2-PPy-S cathode was tested by cyclic voltammetric measurements at the scan rate of 0.1 mV/s from 1.7 V to 2.8 V for 5 cycles. From Figure 7a, the electrode was swept from open circuit voltage (OCV) to 1.7 V, where element sulfur was reduced to Li_2S_2/Li_2S. Notably, the

Li_2S_2/Li_2S species were not oxidized back to element sulfur during the charging process[43,44]. Two well-defined cathodic peaks appeared at ca. 2.3 V (peak i) and 2.1 V (peak ii), which might be ascribed to the reduction of high-order lithium polysulfides (e.g., Li_2S_8) to the low-order species (Li_2S_x. $4 \leqslant x \leqslant 8$), and the transformation of soluble lithium polysulfides to solid Li_2S_2/Li_2S, respectively [23,36]. In the corresponding anodic scan, two adjacent peaks can be identified at 2.3 V (peak iii) and 2.4 V (peak iv), likely due to the conversion of the Li_2S_2/Li_2S to low-order lithium polysulfides and then to high-order polysulfides, respectively [34]. In the following four cycles, the voltammograms overlapped with each other, demonstrating good cycling stability of the electrode.

Electrochemical impedance measurements of the MnO_2-PPy-S electrode were then performed to examine the reaction dynamics for lithium insertion and extraction during the cycling tests. The Nyquist plots are depicted in Figure 7b. It can be seen that the sample exhibited two depressed semicircles in the high and middle frequency domains and a short inclined line in the low frequency domain. The semicircle in the high frequency region can be ascribed to the interfacial charge transfer while the semicircle in the middle frequency region is likely caused by mass transport for the formation of solid polysulfides (Li_2S and Li_2S_2), which disappeared in the subsequent cycles as the Li_2S_2/Li_2S were not converted back to element sulfur, consistent with results from the CV measurements (Figure 7a) [34,43,44] . Meanwhile, the typical Nyquist plots after 100 cycles exhibited a depressed semicircle in the high frequency region and an inclined line in the low frequency region, which likely reflected the charge-transfer

resistance of the interface between the electrolyte and sulfur electrode and the lithium ion semi-infinite diffusion, respectively.

In addition, the resulting MnO_2-PPy-S cathodes demonstrated a remarkable long cycling stability (586 mAh/g after 500 cycles), rate capability (470 mAh/g at 5C) and coulombic efficiency (average 95.7%) due to the fine structural combination of metal oxides (MnO_2) and conducting polymer (PPy) which accommodate the volumetric changes and confine the soluble polysulfides. The electrode performance was higher than leading results reported in recent literature (Table 1).

Table 1. Electrochemical performance of MnO_2/S cathodes of lithium sulfur batteries.

Cathode material	Sulfur content	Cycling stability	Ref.
Hollow PPy-MnO_2-S	74.25%	714 mAh/g at 0.2 C after 200 cycles	[36]
PPy-MnO_2-S	70%	985 mAh/g at 0.2 C after 200 cycles	[37]
rGO-MnO_2-S aerogel	67%	886.7 mAh/g at 0.2 C after 200 cycles	[45]
Hollow carbon nanoboxes-MnO_2 -S	67.9%	496 mAh/g at 4 A/g after 200 cycles	[46]
MnO_2/CMK-S	73.4%	600 mAh/g at 0.1 C after 100 cycles	[47]
Carbon nanofibers-δMnO_2-S	70%	856.1 mAh/g at 0.5 C after 200 cycles	[48]
PPy-MnO_2 nanotubes-S	71%	586 mAh/g at 0.2 C after 500 cycles	This work

4. Conclusion

In this study, a functional nanocomposite was prepared where polypyrrole modified MnO_2 nanotubes were used as a host scaffold for the impregnation of sulfur. The resulting composites showed a high-performance as the cathode material for

lithium sulfur batteries, featuring high specific capacity, excellent cycling stability and good rate capabilities. This was ascribed to the hollow interior of the MnO_2 nanotubes that accommodated the high loading and large volumetric expansion of sulfur particles, and the polypyrrole layer that facilitated charge transfer during the charging-discharging processes.

Acknowledgments

This work was supported by the Natural Science Foundation of Gansu Province (Grant no. 1606RJYA249) and the Fundamental Research Funds for Central Universities (Grant no. lzujbky-2015-271). S.W.C. acknowledged support by the US National Science Foundation (CHE-1710408 and CBET-1848841). W.L.W. was supported by a research fellowship from the China Scholarship Council.

References

(1) Ma, L.; Hendrickson, K. E.; Wei, S.; Archer, L. A. Nanomaterials: Science and applications in the lithium–sulfur battery. *Nano Today* **2015**, *10*, 315-338.

(2) Xu, G.; Ding, B.; Pan, J.; Nie, P.; Shen, L.; Zhang, X. High performance lithium–sulfur batteries: advances and challenges. *Journal of Materials Chemistry A* **2014**, *2*, 12662.

(3) Bruce, P. G.; Freunberger, S. A.; Hardwick, L. J.; Tarascon, J. M. Li-O2 and Li-S batteries with high energy storage. *Nature materials* **2011**, *11*, 19-29.

(4) Ji, X.; Nazar, L. F. Advances in Li–S batteries. *Journal of Materials Chemistry* **2010**, *20*, 9821.

(5) Ligui Li, Jingping Yu, Nan Wang, Jun Zhao, Bin Fan, Shuaibo Zeng, Shaowei Chen, "Structural Engineering of Cathode Materials for Lithium-Sulfur Batteries", in Inorganic Battery Materials (eibc2687), Wiley, 2018

(6) Zeng, S.; Li, L.; Xie, L.; Zhao, D.; Zhou, N.; Wang, N.; Chen, S. Graphene-supported highly crosslinked organosulfur nanoparticles as cathode materials for high-rate, long-life lithium-sulfur battery. *Carbon* **2017**, *122*, 106-113.

(7) Zeng, S.; Li, L.; Zhao, D.; Liu, J.; Niu, W.; Wang, N.; Chen, S. Polymer-Capped Sulfur Copolymers as Lithium–Sulfur Battery Cathode: Enhanced Performance by Combined Contributions of Physical and Chemical Confinements. *The Journal of Physical Chemistry C* **2017**, *121*, 2495-2503.

(8) Chung, S. H.; Manthiram, A. Carbonized eggshell membrane as a natural polysulfide reservoir for highly reversible Li-S batteries. *Advanced materials* **2014**, *26*, 1360-1365.

(9) Wang, Z.; Dong, Y.; Li, H.; Zhao, Z.; Wu, H. B.; Hao, C.; Liu, S.; Qiu, J.; Lou, X. W. Enhancing lithium-sulphur battery performance by strongly binding the discharge products on amino-functionalized reduced graphene oxide. *Nature communications* **2014**, *5*, 5002.

(10) Huang, J. Q.; Zhuang, T. Z.; Zhang, Q.; Peng, H. J.; Chen, C. M.; Wei, F. Permselective graphene oxide membrane for highly stable and anti-self-discharge lithium-sulfur batteries. *ACS nano* **2015**, *9*, 3002-3011.

(11) Liang, X.; Wen, Z.; Liu, Y.; Wu, M.; Jin, J.; Zhang, H.; Wu, X. Improved cycling performances of lithium sulfur batteries with LiNO3-modified electrolyte. *Journal of Power Sources* **2011**, *196*, 9839-9843.

(12) Liu, S.; Li, G. R.; Gao, X. P. Lanthanum Nitrate As Electrolyte Additive To Stabilize the Surface Morphology of Lithium Anode for Lithium-Sulfur Battery. *ACS applied materials & interfaces* **2016**, *8*, 7783-7789.

(13) Li, Z.; Huang, Y.; Yuan, L.; Hao, Z.; Huang, Y. Status and prospects in sulfur–carbon composites as cathode materials for rechargeable lithium–sulfur batteries. *Carbon* **2015**, *92*, 41-63.

(14) Li, W.; Zhang, Q.; Zheng, G.; Seh, Z. W.; Yao, H.; Cui, Y. Understanding the role of different conductive polymers in improving the nanostructured sulfur cathode performance. *Nano letters* **2013**, *13*, 5534-5540.

(15) Xi, K.; Cao, S.; Peng, X.; Ducati, C.; Kumar, R. V.; Cheetham, A. K. Carbon with hierarchical pores from carbonized metal-organic frameworks for lithium sulphur batteries. *Chemical communications* **2013**, *49*, 2192-2194.

(16) Ding, B.; Yuan, C.; Shen, L.; Xu, G.; Nie, P.; Lai, Q.; Zhang, X. Chemically tailoring the nanostructure of graphenenanosheets to confine sulfur for high-performance lithium-sulfur batteries. *J. Mater. Chem. A* **2013**, *1*, 1096-1101.

(17) Chen, R.; Zhao, T.; Lu, J.; Wu, F.; Li, L.; Chen, J.; Tan, G.; Ye, Y.; Amine, K. Graphene-based three-dimensional hierarchical sandwich-type architecture for high-performance Li/S batteries. *Nano letters* **2013**, *13*, 4642-4649.

(18) Wang, H.; Yang, Y.; Liang, Y.; Robinson, J. T.; Li, Y.; Jackson, A.; Cui, Y.; Dai, H. Graphene-wrapped sulfur particles as a rechargeable lithium-sulfur battery cathode material with high capacity and cycling stability. *Nano letters* **2011**, *11*, 2644-2647.

(19) Zu, C.; Fu, Y.; Manthiram, A. Highly reversible Li/dissolved polysulfide batteries with binder-free carbon nanofiber electrodes. *Journal of Materials Chemistry A* **2013**, *1*, 10362.

(20) Jayaprakash, N.; Shen, J.; Moganty, S. S.; Corona, A.; Archer, L. A. Porous hollow carbon@sulfur composites for high-power lithium-sulfur batteries. *Angewandte Chemie* **2011**, *50*, 5904-5908.

(21) Cheng, X.-B.; Huang, J.-Q.; Zhang, Q.; Peng, H.-J.; Zhao, M.-Q.; Wei, F. Aligned carbon nanotube/sulfur composite cathodes with high sulfur content for lithium–sulfur batteries. *Nano Energy* **2014**, *4*, 65-72.

(22) Guo, J.; Xu, Y.; Wang, C. Sulfur-impregnated disordered carbon nanotubes cathode for lithium-sulfur batteries. *Nano letters* **2011**, *11*, 4288-4294.

(23) Wei, W.; Du, P.; Liu, D.; Wang, Q.; Liu, P. Facile one-pot synthesis of well-defined coaxial sulfur/polypyrrole tubular nanocomposites as cathodes for long-cycling lithium-sulfur batteries. *Nanoscale* **2018**, *10*, 13037-13044.

(24) Sun, Y.; Wang, S.; Cheng, H.; Dai, Y.; Yu, J.; Wu, J. Synthesis of a ternary polyaniline@acetylene black-sulfur material by continuous two-step liquid phase for lithium sulfur batteries. *Electrochimica Acta* **2015**, *158*, 143-151.

(25) Li, H.; Sun, M.; Zhang, T.; Fang, Y.; Wang, G. Improving the performance of PEDOT-PSS coated sulfur@activated porous graphene composite cathodes for lithium–sulfur batteries. *J. Mater. Chem. A* **2014**, *2*, 18345-18352.

(26) Wei Seh, Z.; Li, W.; Cha, J. J.; Zheng, G.; Yang, Y.; McDowell, M. T.; Hsu, P. C.; Cui, Y. Sulphur-TiO2 yolk-shell nanoarchitecture with internal void space for long-cycle lithium-sulphur batteries. *Nature communications* **2013**, *4*, 1331.

(27) Liang, X.; Nazar, L. F. In Situ Reactive Assembly of Scalable Core-Shell Sulfur-MnO2 Composite Cathodes. *ACS nano* **2016**, *10*, 4192-4198.

(28) Dai, C.; Hu, L.; Wang, M.-Q.; Chen, Y.; Han, J.; Jiang, J.; Zhang, Y.; Shen, B.; Niu, Y.; Bao, S.-J.; Xu, M. Uniform α-Ni(OH)2 hollow spheres constructed from ultrathin nanosheets as efficient polysulfide mediator for long-term lithium-sulfur batteries. *Energy Storage Materials* **2017**, *8*, 202-208.

(29) Xu, G.; Ding, B.; Shen, L.; Nie, P.; Han, J.; Zhang, X. Sulfur embedded in metal organic framework-derived hierarchically porous carbon nanoplates for high performance lithium–sulfur battery. *Journal of Materials Chemistry A* **2013**, *1*, 4490.

(30) Wu, H. B.; Wei, S.; Zhang, L.; Xu, R.; Hng, H. H.; Lou, X. W. Embedding sulfur in MOF-derived microporous carbon polyhedrons for lithium-sulfur batteries. *Chemistry* **2013**, *19*, 10804-10808.

(31) Wang, S.; Yang, Z.; Zhang, H.; Tan, H.; Yu, J.; Wu, J. Mesoporous β-MnO2/sulfur composite as cathode material for Li–S batteries. *Electrochimica Acta* **2013**, *106*, 307-311.

(32) Liang, X.; Hart, C.; Pang, Q.; Garsuch, A.; Weiss, T.; Nazar, L. F. A highly efficient polysulfide mediator for lithium-sulfur batteries. *Nature communications* **2015**, *6*, 5682.

(33) Wang, X.; Li, G.; Li, J.; Zhang, Y.; Wook, A.; Yu, A.; Chen, Z. Structural and chemical synergistic encapsulation of polysulfides enables ultralong-life lithium–sulfur batteries. *Energy & Environmental Science* **2016**, *9*, 2533-2538.

(34) Ni, L.; Wu, Z.; Zhao, G.; Sun, C.; Zhou, C.; Gong, X.; Diao, G. Core-Shell Structure and Interaction Mechanism of gamma-MnO2 Coated Sulfur for Improved Lithium-Sulfur Batteries. *Small* **2017**, *13*.

(35) Li, W.; Yao, H.; Yan, K.; Zheng, G.; Liang, Z.; Chiang, Y. M.; Cui, Y. The synergetic effect of lithium polysulfide and lithium nitrate to prevent lithium dendrite growth. *Nature communications* **2015**, *6*, 7436.

(36) Li, Y.; Shi, B.; Liu, W.; Guo, R.; Pei, H.; Ye, D.; Xie, J.; Kong, J. Hollow polypyrrole @ MnO 2 spheres as nano-sulfur hosts for improved lithium-sulfur batteries. *Electrochimica Acta* **2018**, *260*, 912-920.

(37) Zhang, J.; Shi, Y.; Ding, Y.; Zhang, W.; Yu, G. In Situ Reactive Synthesis of Polypyrrole-MnO2 Coaxial Nanotubes as Sulfur Hosts for High-Performance Lithium-Sulfur Battery. *Nano letters* **2016**, *16*, 7276-7281.

(38) Wang, J.-G.; Yang, Y.; Huang, Z.-h.; Kang, F. MnO_2/polypyrrole nanotubular composites: reactive template synthesis, characterization and application as superior electrode materials for high-performance supercapacitors. *Electrochim. Acta* **2014**, *130*, 642-649.

(39) Luo, J.; Zhu, H. T.; Fan, H. M.; Liang, J. K.; Shi, H. L.; Rao, G. H.; Li, J. B.; Du, Z. M.; Shen, Z. X. Synthesis of single-crystal tetragonal α-MnO_2 nanotubes. *J. Phys. Chem. C* **2008**, *112*, 12594-12598.

(40) Liang, X.; Zhang, M.; Kaiser, M. R.; Gao, X.; Konstantinov, K.; Tandiono, R.; Wang, Z.; Liu, H.-K.; Dou, S.-X.; Wang, J. Split-half-tubular polypyrrole@sulfur@polypyrrole composite with a novel three-layer-3D structure as cathode for lithium/sulfur batteries. *Nano Energy* **2015**, *11*, 587-599.

(41) Ma, G.; Wen, Z.; Jin, J.; Lu, Y.; Rui, K.; Wu, X.; Wu, M.; Zhang, J. Enhanced performance of

lithium sulfur battery with polypyrrole warped mesoporous carbon/sulfur composite. *Journal of Power Sources* **2014**, *254*, 353-359.

(42) Wang, C.; Wan, W.; Chen, J.-T.; Zhou, H.-H.; Zhang, X.-X.; Yuan, L.-X.; Huang, Y.-H. Dual core–shell structured sulfur cathode composite synthesized by a one-pot route for lithium sulfur batteries. *J. Mater. Chem. A* **2013**, *1*, 1716-1723.

(43) Cai, Y.; Guo, Y.; Jiang, B.; Lv, Y. Encapsulation of cathode in lithium-sulfur batteries with a novel two-dimensional carbon allotrope: DHP-graphene. *Scientific reports* **2017**, *7*, 14948.

(44) <J. Electrochem. Soc.-2004-Mikhaylik-A1969-76.pdf>.

(45) Zhao, X.; Wang, H.; Zhai, G.; Wang, G. Facile Assembly of 3D Porous Reduced Graphene Oxide/Ultrathin MnO2 Nanosheets-S Aerogels as Efficient Polysulfide Adsorption Sites for High-Performance Lithium-Sulfur Batteries. *Chemistry* **2017**, *23*, 7037-7045.

(46) Rehman, S.; Tang, T.; Ali, Z.; Huang, X.; Hou, Y. Integrated Design of MnO2 @Carbon Hollow Nanoboxes to Synergistically Encapsulate Polysulfides for Empowering Lithium Sulfur Batteries. *Small* **2017**, *13*.

(47) Liu, J.; Wang, C.; Liu, B.; Ke, X.; Liu, L.; Shi, Z.; Zhang, H.; Guo, Z. Rational synthesis of MnO 2 @CMK/S composite as cathode materials for lithium–sulfur batteries. *Materials Letters* **2017**, *195*, 236-239.

(48) Lai, Y.; Wang, P.; Qin, F.; Xu, M.; Li, J.; Zhang, K.; Zhang, Z. A carbon nanofiber@mesoporous δ-MnO2 nanosheet-coated separator for high-performance lithium-sulfur batteries. *Energy Storage Materials* **2017**, *9*, 179-187.